ChemComm

FEATURE ARTICLE

View Article Online
View Journal | View Issue

Cite this: *Chem. Commun.*, 2015, **51**, 8213

Fouling in microstructured devices: a review

M. Schoenitz,[a] L. Grundemann,[b] W. Augustin*[a] and S. Scholl[a]

Received 4th October 2014,
Accepted 24th February 2015

DOI: 10.1039/c4cc07849g

www.rsc.org/chemcomm

Microstructured devices are widely used for manufacturing products that benefit from process intensification, with pharmaceutical products or specialties of the chemical industry being prime examples. These devices are ideally used for processing pure fluids. Where particulate or non-pure flows are involved, processes are treated with utmost caution since related fouling and blocking issues present the greatest barrier to operating microstructured devices effectively. Micro process engineering is a relatively new research field and there is limited understanding of fouling in these dimensions and its underlying processes and phenomena. A comprehensive review on fouling in microstructured devices would be helpful in this regard, but is currently lacking. This paper attempts to review recent developments of fouling in micro dimensions for all fouling categories (crystallization, particulate, chemical reaction, corrosion and biological growth fouling) and the sequential events involved (initiation, transport, attachment, removal and aging). Compared to fouling in macro dimensions, an additional sixth category is suggested: clogging by gas bubbles. Most of the reviewed papers present very specific fouling investigations making it difficult to derive general rules and parameter dependencies, and comparative or critical considerations of the studies were difficult. We therefore used a statistical approach to evaluate the research in the field of fouling in microchannels.

Introduction

Process intensification is important for the chemical industry because it can help increase efficiency in both ecological and economic terms. Stankiewicz *et al.*[1] emphasized the significance of process intensification by describing it as a "paradigm shift" for process and equipment design. Micro process engineering includes hybrid unit operations and miniaturization, as well as widely applied process intensification technologies such as structured catalysts and packings.

An intensifying process employing a microstructure device is associated with at least one process that occurs at a dimension below 1 mm, and consequently results in very high surface-to-volume ratios. Laminar flow typically results from the combination of characteristic dimensions in the μ-scale and flow velocities that are frequently limited by an acceptable pressure drop. This means low shear stresses are exerted on the fluid. Applied miniaturization also leads to short transport lengths for heat and mass transfer as well as low residence times that

[a] *Institute for Chemical and Thermal Process Engineering, Technische Universität Braunschweig, Langer Kamp 7, Braunschweig, Germany. E-mail: w.augustin@tu-braunschweig.de*
[b] *Creavis, Evonik Industries AG, Marl, Germany*

M. Schoenitz

Martin Schoenitz is a doctoral researcher at the Institute for Chemical and Thermal Process Engineering, Technische Universität Braunschweig, Germany. In 2010 he received his Dipl.-Ing. degree from Technische Universität Braunschweig. He is currently working on the transfer of pharmaceutical macro-batch processes to continuous processes in microstructured devices with a focus on fouling phenomena.

L. Grundemann

Laura Grundemann is a project manager in the unit 'Sustainable Businesses' at Creavis, the strategic innovation unit of Evonik located in Marl, Germany. She received her Dr.-Ing. from the Technische Universität Braunschweig. Her current work focuses on managing and controlling innovation projects while taking economic, environmental as well as social aspects into account.

can positively affect a wide range of applications. In particular, reactions with fast kinetics, reactions initiated by mixing events or highly temperature sensitive reactions are especially likely to benefit.[2] This applies to existing processes for which the advantages are being investigated by companies like BASF and DuPont.[3] Likewise, micro process engineering may act as a "process enabler" in situations where the creation of completely new processing routes in micro structures can render production economically viable, having formerly been not feasible in macroscale equipment.[2,4]

The benefits are, however, at the expense of lower capacities compared to macro equipment. Microstructured devices are therefore suited for products with maximum capacities of 100–1000 t/a: that is, specialties or products of the pharmaceutical industry.[5] Particulate flows are another challenge for microstructured devices since the ratio of the characteristic dimension to the particle diameter decreases significantly. This is one of the reasons why fouling – *i.e.*, the unwanted deposition on surfaces – and plugging occur regularly in microstructured devices. The consequences for process performance can be dramatic: fouling layers lead to local constrictions that change flow velocities and increase pressure drops. In microstructured devices with internal numbering-up, *i.e.*, multi-channel apparatuses, maldistributions of the flow can result in spatial and time distribution of relevant process parameters. In the worst case, complete blockages of the microchannels can occur.

Fouling in general is a well-known problem, and one that has been encountered ever since our ancestors domesticated fire.[6] Fouled layers cause high financial losses in all industry sectors due to increased transport and installation costs, capital costs for antifouling equipment, fuel costs, maintenance costs and due to production losses.[7] In Germany, the loss is equivalent to 0.25% of the gross domestic product, or about six billion €/a. Fouling can also lead to high capital expenditure. For example, heat exchangers have been reportedly oversized by 30% on average to compensate for fouling.[7] A desire to overcome such costs have therefore led to increased research efforts to understand macro-scale fouling phenomena.[8–13]

A comprehensive overview on fouling was first described by Epstein[14] in 1983 using a 5 × 5 matrix which was based on the five primary fouling categories and the five successive events during the formation of fouling layers. 26 years later, Wilson updated the matrix and his analysis indicated that progress had been made for all research topics.[15]

Conversely, fouling in microstructured devices and the underlying phenomena in the dimensions of $\leq$1000 μm have only been investigated sparsely so far. Although fouling had already been identified by Hessel *et al.*[16] in 2004 as a major barrier to the successful implementation of microstructured devices, only a few research projects have focused on the topic in the subsequent years. These projects led to some very basic design rules and rules of thumb to prevent fouling, such as the design of channels "as small as necessary and beneficial, not as small as possible".[17] Wiles and Watts[18] refined that rule for particulate systems and from three examples concluded that plugging occurs when the particle size is larger than 10% of the smallest dimension in the system. Despite all efforts, Hartman stated in 2012 that plugging was still the greatest challenge to the design of continuous processes using micro structured devices.[4] This work aims to comprehensively review and assess fouling and plugging in microstructured devices for better understanding of the underlying phenomena, and to enable more efficient equipment design. For structuring purposes, the 5 × 5 matrix invented by Epstein[14] for macro-scale processes is applied for the microstructured systems. Membrane fouling is, however, excluded from this review for it differs significantly from microchannels due to the porous nature of the fouling surface combined with the influence of transmembrane flow on the fouling process.[19]

Classification of fouling

Fouling phenomena in macro-scale devices were divided into five different categories by Epstein[14] according to the cause of fouling and the type of matter that consequentially attaches to

W. Augustin

Wolfgang Augustin is a senior researcher at the Institute for Chemical and Thermal Process Engineering, Technische Universität Braunschweig, Germany. He received his Dr.-Ing. in 1992 from Technische Universität Braunschweig. His main research interests are heat and mass transfer, fouling, viscous fluid flow, and surface interactions on the micro scale level.

S. Scholl

Stephan Scholl is professor of Chemical and Thermal Process Engineering and head of the respective Institute at the Technische Universität Braunschweig, Germany. He received his doctorate degree in 1991 from the Technical University of Munich. After eleven years with BASF AG, Ludwigshafen, Germany, he joined TU Braunschweig in 2002. His main research areas are sustainable production concepts, innovative equipment technologies, fouling and cleaning, reaction and separation in pharmaceutical as well as biotechnological processes.

	1. Crystallization fouling	2. Particulate fouling	3. Chemical reaction fouling	4. Corrosion fouling	5. Biological growth fouling
1. Initiation	1.1	1.2	1.3	1.4	1.5
2. Transport	2.1	2.2	2.3	2.4	2.5
3. Attachment	3.1	3.2	3.3	3.4	3.5
4. Removal	4.1	4.2	4.3	4.4	4.5
5. Aging	5.1	5.2	5.3	5.4	5.5

Fig. 1 Epstein's 5 × 5 matrix: categories and sequential events of fouling.

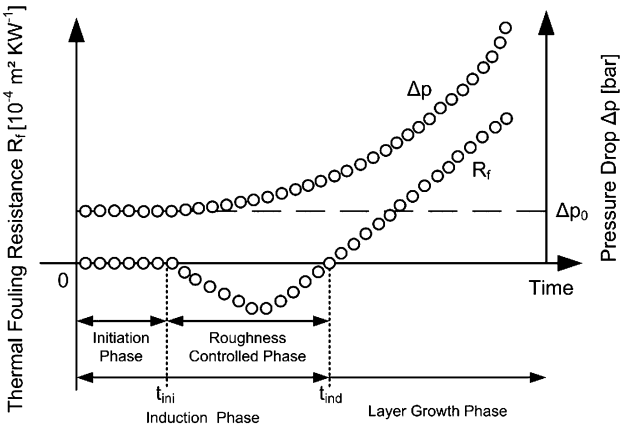

Fig. 2 Graphical definition and schematic development of the thermal fouling resistance and the pressure drop over process time.

the surface, see Fig. 1. "Crystallization fouling" means the crystallization of dissolved salts or freezing of pure liquid or liquid mixtures on surfaces. "Particulate fouling" denotes the deposition of fine particles already present in the reactant streams, whereas "chemical reaction fouling" involves the attachment of solids that form during a chemical reaction, such as polymerization or decomposition. If fouling layers are composed of corrosion products, this is referred to as "corrosion fouling". Micro or macro-organisms attaching to the surface is classified as "biological growth fouling".

In each case, a sequence of five events occurs according to the Epstein model,[14] see Fig. 1. The initiation phase is a delay period before significant fouling can be recorded. During the transport phase, the fouling reactant is transported from the fluid's bulk flow to the surface followed by the attachment of the key component. Once a component is attached, it will either be removed by hydrodynamic forces or aging of the respective fouling layer will start. The aging process consists of crystal or chemical structure changes. For a detailed description of the fouling categories and the sequential events, see Epstein.[14] A 5 × 5 matrix was then compiled by Epstein with fouling categories as column labels and the events as row labels, see Fig. 1.

Heat exchanger fouling

Fouling can occur in any industry sector and in any unit operation. However, it is most common in heat exchangers because fouling is often a temperature-sensitive process. In these devices, fouling can be quantified by two key parameters: the thermal fouling resistance R_f and the pressure drop Δp, representing the volume- and ultimately mass-based fouling resistance. The mechanisms of fouling in macro heat exchangers and the development of R_f are well established.[14] R_f is calculated by subtracting the reciprocal heat transfer coefficient of the non-soiled surface (k_0) from the reciprocal heat transfer coefficient of the soiled surface (k_f), see eqn (1). Based on this value, the degree of fouling can be classified for macro dimensions according to Table 1.

$$R_f = \frac{1}{k_f} - \frac{1}{k_0} \quad (1)$$

As the second key parameter, the mass-based fouling resistance refers to the attached mass as detected by the pressure drop across the heat exchanger. The fouling process is divided into several phases, see Fig. 2. The initiation phase is characterized by a thermal fouling resistance of R_f = 0 m^2 K W^{-1} and ends after the initiation time t_{ini}. Starting from that point, matter first attaches to the technical surface which leads to an enhanced heat transfer at the beginning and therefore a negative value of R_f. This phase is called the roughness controlled phase and together with the preceding initiation phase, forms the induction phase. It ends after the induction time t_{ind} and is followed by the layer growth phase as shown in Fig. 2. It has been shown by Albert *et al.*[20] that a proper accounting of roughness and constriction effects may eliminate negative values of the thermal fouling resistance in macro scale. This provides the basis for a consistent relation between the thermal- and the mass-based fouling resistance. One of the core questions is whether the problem depicted in Fig. 2 also holds for micro system fouling.

Table 1 Classification of fouling for macro dimensions

Fouling classification	Thermal fouling resistance R_f [m^2 K W^{-1}]
No/low	$0\ldots2 \times 10^{-4}$
Moderate	$3\ldots9 \times 10^{-4}$
Severe	$\geq 10 \times 10^{-4}$

Experimental Fouling Investigstions in Microchannels

Crystallization fouling

Crystallization fouling, where the underlying process is crystallization out of a solution and not the crystallization of a bulk-phase, is caused by heterogeneous crystallization, *i.e.*, the nucleation of ion pairs on solid surfaces and the subsequent growth of crystals until a crystal layer is formed. Homogenous crystallization by contrast is characterized by nuclei, and ultimately

crystals, forming in the solution, *e.g.*, in the bulk of a fluid flow. Fouling problems caused by the latter crystallization mechanism are related to particulate fouling and will be addressed in the corresponding section below.

Although only a few papers have explored heterogeneous crystallization in micro devices, some of the work was published quite recently which highlights the importance of this fouling mechanism for the operation of micro devices. All of the papers covered crystallization fouling in micro heat exchangers where the micro roughness of the heat transfer surface, such as found at grain boundaries, serve as nucleation sites. The driving force for the formation of crystals is supersaturation in the vicinity of the heated wall. Table 2 lists published works into crystallization fouling in micro devices, specifying in each case the characteristic dimensions (number of channels, width × height × length) of the micro heat exchanger, Reynolds number (eqn (2)), and wall temperature, where available. Missing values, denoted in italics, were calculated wherever possible based on the given information.

$$\mathrm{Re} = \frac{\rho d_h u}{\eta} \quad (2)$$

where ρ [kg m^{-3}] is the density, d_h [m] the characteristic dimension, u [m s^{-1}] the velocity and η [Pa s] the dynamic viscosity.

Brandner *et al.*[21] described in very general terms the fouling of $CaCO_3$ in an electrically heated device, which was repeatedly heated up to 80 °C and cooled down. After some time, a significant pressure drop and reduction of heat duty were observed. The apparatus could be regenerated completely by cleaning with citric acid.

Mayer *et al.*[22] used a supersaturated $CaCO_3$ solution in a fluidic heated heat exchanger with one respectively 12 micro channels, operated in counter current flow. They applied six thermocouples in the heat transferring foil to measure the local wall temperature in the flow direction. The flow rate was varied within the laminar flow regime. At low flow rates, the heat flow was reduced by over 50% due to fouling, whereas it decreased by only 27% at higher flow rates. The pressure drop increased up to 60 times compared to the initial value at low flow rates. Fouling was especially intense at the outlet of the salt solution because of the higher temperatures present. Visual observations showed no removal of any fouling. This corresponds with a relatively low calculated wall shear stress compared to the adhesive strength of the crystals on the heat exchanger surface. In all experiments an induction period and an asymptotic behavior, described by a constant R_f after a specific time, were noticed at the beginning and towards the end of a test, respectively.

An asymptotic behavior, *i.e.*, a decrease of the slope of the fouling curve (R_f), can be attributed to gradually decreasing supersaturation due to changing surface temperature in the course of fouling layer formation. The same micro heat exchanger and salt system was used by Bucko *et al.*,[23] with the difference that the Reynolds number and wall temperature were varied. For some experiments they detected a negative value for the fouling resistance during the induction period, which is equivalent to that found in macroscopic heat exchangers, see Fig. 2. The induction time was reduced with increasing wall temperature, flow velocity and salt concentration. Again, removal of crystals was not observed. In later experiments, Mayer *et al.*[24] observed *via* optical investigation an uneven distribution of the deposits in the parallel channel arrangement which had developed during the experiment. This was due to an inhomogeneous distribution of the heat flux and to a fouling-induced maldistribution of the fluid flow in the parallel channels.

In order to model the kinetics of the crystallization in the above mentioned micro heat exchanger, Bucko *et al.*[23] calculated the Hatta and Damköhler numbers on the basis of experimental data. The Hatta number describes the correlation between reaction velocity and mass transport and was found to be <0.3 indicating that the process is reaction-controlled. The same conclusions were drawn from the Damköhler number which is the ratio of reaction rate to diffusion rate. Values $\ll 1$ exclude a mass transport-controlled deposition of $CaCO_3$. The temperature dependency was described with the help of an Arrhenius approach and the results were in good agreement with literature data. The kinetics of fouling in a micro heat exchanger with a cross flow arrangement was studied and modelled by Mayer *et al.*[25] They determined the thermal fouling resistance by temperature measurements and the mass-based fouling resistance by measuring the pressure drop. Additionally, they determined the surface coverage of the $CaCO_3$ deposits in the micro channels with a digital microscope. Correlating these results with the determined fouling resistance values showed that the surface coverage rate was a good estimate of the fouling behavior of salt solutions in micro devices. A threshold for the transition from the induction to the crystal growth period was defined on that basis.

Different coatings and their influence on fouling mechanism in laminar flow regimes were studied by Benzinger *et al.*[26] However, the diamond like carbon (DLC) and fluorinated ethylene propylene (FEP) coatings did not lead to any significant changes compared to fouling studies conducted with uncoated stainless steel (316L) devices as reference.

Cleaning in place (CIP) experiments of micro heat exchangers with $CaCO_3$ crystal fouling layers were carried out with HCl solution by Mayer *et al.*[24] Visual observations revealed that cleaning progressed very quickly after the first channels had been freed from deposits. The CIP procedure might have also

Table 2 References of experimental work on crystallization fouling in micro heat exchangers: all experiments were realized with $CaCO_3$. Numbers in italics denote calculations performed by the authors based on the information provided in the paper. n_{mc} = number of microchannels, d_h = characteristic dimension or channel dimensions, Re = Reynolds number, T_w = wall temperature

Ref.	n_{mc} [—]	d_h [μm]	Re [—]	T_w [°C]
Benzinger (2005)[27]	22	800 × 100 × 22 000	*142*	96
Benzinger (2007)[26]	2, 17	800 × 100 × 25 000	110–2540	99
Brandner (2007)[21]	17	*178*	110	99
Mayer (2012)[22]	1, 12	400 × 200 × 24 000	66–792	76
Bucko (2012)[23]	12	400 × 200 × 24 000	42–145	65–88
Mayer (2013)[24]	1, 12, 18	400 × 200 × 24 000	79–792	70–83
Mayer (2015)[25]	33	400 × 400 × 19 600	51–507	*78*

been enhanced by bypass flows below the strips separating the different microchannels from each other, which were enabled by the clamped design of the micro heat exchanger. Nevertheless, the cleaning experiments were fairly reproducible. Another *in situ* cleaning method, the application of ultrasound, was investigated by Benzinger *et al.*[27] in an electrically heated micro heat exchanger. After the outlet temperature of the salt solution had dropped by 15 K due to $CaCO_3$ fouling, an ultrasonic pulse of 1 min was applied. In this manner, the starting temperature was achieved. The power level was, however, too low to generate cavitation, so the cleaning effect resulted from acoustic micro streaming near the solid/liquid interface. In the following cycles, the heat flow rate decreased at an ever faster rate after each sonic treatment. Optical observations indicated that this was due to remaining crystals in the micro channels.

Chemical reaction fouling

Chemical reaction fouling occurs when chemical reactions with wall materials (*e.g.* polymerization, decomposition) or the reactants of such processes lead to the deposition of solids.[8,14] No published work, however, was found for the above definition of chemical reaction fouling as it applies to processes in microstructured devices, because fouling from chemical reactions with solid products conducted in microstructured devices with inert wall materials is classified as particulate fouling, which is addressed below.

Particulate fouling

Particulate fouling, potentially occurring when suspensions or particle-laden fluid flows are processed, was the most common fouling category according to our search. Investigations dealing with particulate fouling in micro devices are listed in Table 3. The information includes the type of particles present, their diameter and characteristic dimension, and Reynolds number. When these parameters were not stated explicitly in the papers, they were calculated based on the given information and are present in italics in the table.

Papers referred to in Table 3 that also contain experimental work are discussed in the remainder of this chapter. Hartman[4] worked out three hydrodynamic mechanisms that lead to particulate fouling in micro devices: constrictions, bridging and random detachment of deposits. The following chapter is

Table 3 References of experimental work on particulate fouling in microstructured devices. Numbers in italics denote calculations performed by the authors, based on information provided in the papers. d_h = characteristic dimension, d_p = particle diameter, Re = Reynolds number

Ref.	Particles	d_h [μm]	d_p [μm]	Re [—]
Niida (1989)[35]	Polystyrene latex, iron oxide	730	1–15, 0.3, 0.73	32–8200
Yiantsios (1998)[38]	Glass	670	1.8	33–89
Yiantsios (1995)[36]	Glass	670	2–15	4.2–5200
Vacassy (2000)[50]	$CaCO_3$	4000	*<20*	*<10*
Schenk (2001)[56]	$CaCO_3$	*107*		*60*
Werner (2002)[45]	Different types of reactions and micromixers			
Jongen (2003)[51]	$CaCO_3$, $BaTiO_3$		*<3*	
Yiantsios (2003)[37]	Glass and silica	460–670	0.9–1.8	33–89
Wille (2004)[5]	Azo-pigments	1000		*Turbulent*
Shestopalov (2004)[48]	Colloidal CdS	50		*<10*
Takagi (2004)[42]	Titanium	3000		
Wagner (2005)[40]	Gold	*170–260*	0.005–0.05	*50–800*
Kockmann (2005)[3]	Aerosol	461	0.010–0.850	417
Heim (2006)[28]	Aerosol	Numerical simulation of experimental results from Kockmann[3]		
Přibyl (2005)[55]	$CaCO_3$	*500*		*Diffusive mixing*
Sharp (2005)[63]	Polystyrene latex	75–400	22–136	15–600
Gerdts (2006)[52]	Protein	*~200*	*<200*	
Perry (2006)[32]	Silica	106	3–10	18.4
Poe (2006)[49]	Indigo	*1600*		*~100*
Nagasawa (2006)[47]	Silver halide particles	100	<0.1	*400–10 000*
Heinzel (2007)[62]	Polystyrene spheres	100–285	0.7	
Sotowa (2007)[53]	$CaCO_3$, silver	500	<1	*<10*
Perry (2008)[31]	Silica	225	Si: 4	17
	Alumina		Al: 1.25	
Perry (2008)[33]	Al_2O_3	220, 225	0.248–24	17–41
Kockmann (2008)[2]	Barium sulfate	400	0.25	300–500
Shukla (2009)[39]	Glass spheres	230	115–218	<0.1
Marmiroli (2009)[43]	$CaCO_3$	*17*		*<150*
Georgieva (2010)[65]	Latex dispersions	10–26	0.1–0.14	<1
Génot (2010)[44]	Organic nanocrystals	15	50–110	*<1*
Horie (2010)[54]	Maleic anhydride	500–1600		*~1000*
Sedelmeier (2010)[59]	Manganese dioxide	500		
Hartman (2010)[57]	Aryl chloride	400	400	*<5*
Genovese (2011)[30]	PMMA	100	2.3	
Noël (2011)[58]	Aryl chloride	400	400	*<5*
Chowdhury (2012)[34]	TiO_2	160	0.7–1.2	<1
Grundemann (2012)[46]	Ink agglomerates	600	0.1–2	*<1000*
Zhengying (2012)[41]	Sand	1100–1800	100–300	
Schoenitz (2014)[66]	Lipid	200	0.3	30

subdivided accordingly. Since papers describing aerosol-based fouling and blocking issues in microstructured devices are published very rarely, they are discussed in the following paragraph, independently from the above stated three hydrodynamic mechanisms. All other papers deal with particle-laden liquids.

Aerosol based particulate fouling in microstructured devices. Particle deposition caused by aerosol particles was studied by Kockmann *et al.*[3] They investigated the deposition of monodisperse aerosol particles (NaCl and vitamin E acetate) in a T-shaped micro-mixer with a rectangular channel. From the passing probability of the particles they determined three particle diameter classes. For small particles ($d_p < 30$ nm), a diffusion-controlled attachment to the wall was observed. Large particles ($d_p > 200$ nm) showed a drastic decrease in their passing probability through the T-shaped micro-mixer due to increasing mass and accordingly, inertia-controlled attachment to the walls. Fouling was especially prominent at sharp bends. For particles with diameters of 30 nm $\leq d_p < 200$ nm, a passing probability of nearly 100% was found. Kockmann *et al.*[3] combined these results with the dimensionless Peclet (eqn (3)) and Stokes numbers (eqn (4)). To avoid aerosol particle deposition by diffusion, a Peclet number below 5×10^6 was suggested:

$$\mathrm{Pe} = \frac{t_D}{t_F} = \frac{u d_h}{d_p} \quad (3)$$

where t_D [s] is the characteristic diffusion time, t_F [s] the characteristic flow time, u [m s^{-1}] the flow velocity, d_h [m] the characteristic dimension and d_p [m] the particle diameter.

$$\mathrm{Stk} = \frac{t_P}{t_F} = \frac{\rho_p {d_p}^2 u}{18\eta d_h} \quad (4)$$

where t_P [s] is the particle relaxation time, ρ_P [kg m^{-3}] the particle density and η [Pa s] the dynamic viscosity.

A Stokes number below 0.05 is recommended to prevent aerosol particle deposition by inertia.[3] These experiments were compared with fluid dynamic simulations of the micro-mixer by Heim *et al.* and showed good agreement.[28] Bell and Groll[29] also investigated fouling caused by aerosols passing different types of dust through several plate-fin heat exchangers with spacings between the fins of 2 mm, 1.3 mm and 1 mm. In general, smaller spacings resulted in higher particulate fouling.[29]

Constrictions/small dimensions

General influence of constrictions. The sudden enlargement or narrowing of channels are unavoidable when microstructured devices are designed to form an integral part of a process chain. They are present at the device's entrance or exit or even within the micro device, for instance in flow distribution headers. When the cross-sectional flow path is decreased, lift forces acting on particles change significantly. In the case of gravitational forces dominating the lift forces, particles or agglomerates may sediment and settle down on the microchannel or header walls. Hartman[4] studied constriction-based fouling and estimated the fouling potential *via* inertial impaction by means of the Stokes number (eqn (4)). For Stokes < 1, stable particles (against agglomeration) are prevented from attaching to the wall due to inertial impaction. Genovese and Sprakel[30] investigated the effect of constrictions in microchannels on the flow profile of particulate flows. The velocities and velocity profiles downstream of the constrictions were significantly altered compared to the corresponding upstream patterns. In crystallization processes, this causes extended crystalline particle domains upstream of the constriction. Perry and Kandlikar[31] compared the shear stresses within microchannels with those in the header regions at the device's entrance and exit. The stresses measured in the channels were 11 times higher than in the headers. In the latter, intense fouling occurred due to the dominating gravitational forces. They also performed fouling investigations with alumina particle-laden flows in silicon microchannels used for chip cooling.[32,33] They determined how the involved forces (electrostatic, van der Waals, gravity, lift) (inter-)act during both particle–particle and particle–wall interactions. Employing 24 μm aggregates, they found that fouling occurred at both headers, however not in the microchannels themselves. Again, gravitational forces dominated in the header region, being 24 times higher than the corresponding lift forces. In the microchannels, on the other hand, the lift forces exceeded the gravitational forces by a factor of three, preventing the particles from settling to the microchannel walls. They also showed that the fouling behavior depends on the pH value. Varying pH values correspond to different zeta potential differences between the surface and the alumina particles. In the case of low pH values, the particles were electrostatically attracted to the surface, whereas at high pH values electrostatic repulsion occurred. Near the isoelectric point, the particles were unstable. By switching pH from 5.5 to 10.3, fouling of 3 μm silica particles was mitigated.[32] The particle size also plays an important role in the fouling behavior of particle-laden flows. The authors monitored pressure drop as another indicator for fouling, using 3 μm and 10 μm silica particles. For the smaller particles, they detected a drastic increase of the pressure drop during the experiments, indicating strong fouling. This effect was, however, not measurable for the 10 μm particles. This is due to the considerably lower lift forces in the case of the 3 μm silica particles since the particle size appears to the power of four in the relevant equation. Thus, comparable low lift forces supported movement of the smaller particles to the channel walls. Similar results were found by Chowdhury and Walker[34] when applied to TiO_2 aggregates with a diameter of 0.7 μm to 1.2 μm. Additional to the pH value, they identified the ionic strength and the flow rate as important fouling parameters, of which the pH value was identified as the most influential impact factor.

Critical velocity/particle diameter. The literature describes two methods to determine specific fouling-mitigating parameters. First, the critical velocity is revealed by gradually increasing fluid velocity until attached particles detach again. Second, the critical particle diameter is detected by increasing the particle diameter gradually until fouling occurs. Varying the flow rate as a fouling mitigation tool was investigated in detail by Niida *et al.*[35] The critical velocity for particle removal was determined using aqueous suspensions of polystyrene latex and iron oxide particles in a borosilicate glass cell. They observed the

glass cell with a microscope and were able to count the number of removed particles during cleaning experiments. Having determined the critical velocity, the viscous drag and adhesive forces were calculated with the latter being proportional to the particle diameter.[35]

The influence of varying shear stresses on particle attachment, transport and removal was studied by Yiantsios and Karabelas.[36–38] They performed experiments with glass particles on substrates made of glass and stainless steel. At low shear stress rates, sedimentation-controlled deposition occurred, whereas the lift force gained more influence at increasing shear stress rates. The experimental results were in good agreement with a particle deposition model. In the same way, Shukla and Henthorn[39] investigated the detachment velocity of single glass particles. It increased logarithmically with the ratio between the particle diameter and the characteristic microchannel dimension.

Furthermore, they calculated the forces acting on a single spherical particle and suggested improvements to the model. Wagner and Köhler[40] analyzed the attachment and detachment of synthesized gold nanoparticles with particle diameters in the range of 5–50 nm. However, the microstructured reactor had only been used for short periods of time: enough to produce less than 10 ml gold nanoparticle dispersion. Within these short periods of time gold films or deposits of elementary gold were found inside after processing. This means the reactor surfaces acted as a nucleation starter at low flow rates. However, at higher flow rates, less fouling was observed due to higher shear stress near the surfaces.[40]

The second fouling-preventing method – the determination of the critical diameter of the particles – was studied by Zhengying *et al.*[41] Based on three examples, Wiles and Watts[18] drew the conclusion that blocking by particles occurs in cases where the particle size is larger than 10% of the smallest dimension in the system.

Precipitation experiments. Precipitation is a common application for particulate flows in microstructured devices. It is representative of any other particle synthesis since the reaction conditions and thus the nuclei formation and aggregation processes can be well controlled.[42] Precipitation experiments in microstructured devices frequently result in fouling and blocking issues due to the precipitated particles. Different possibilities to reduce fouling during precipitation experiments in microstructured devices were reported.

Avoiding particle–wall interactions. One way to decrease fouling during precipitation experiments is by reducing particle–wall contacts, for example by using hydrodynamic-focusing micromixers, see Fig. 3. Fluid A enters through both side channels, whereas fluid B enters through the central channel. Fluid A therefore squeezes fluid B, leading to a thin, confined stream along the single outlet channel.

Marmiroli *et al.*[43] reported this technique for the precipitation of calcium carbonate. Particles attached to the walls interfered with particle size measurements using X-ray scattering and even led to channel blockages. The output nozzle had a diameter of 6 μm and the output was 288 μl min^{-1} in total,

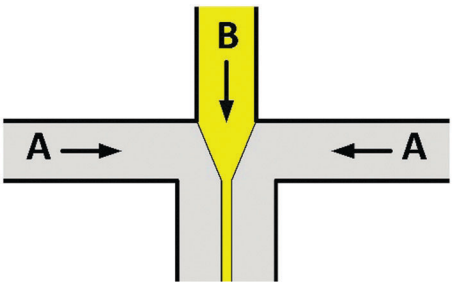

Fig. 3 Schematic of the hydrodynamic-focusing principle. Fluid B is squeezed by fluid A. In fluid B, precipitated particles will have no contact with the microchannel walls.

resulting in a jet velocity of 13 m s^{-1}. Furthermore, the device was specifically designed to prevent recirculation and flow stagnation in front of the nozzle, which had resulted in unwanted particle formation and deposition inside the mixer in previous designs.[43]

Takagi *et al.*[42] also successfully adopted the hydrodynamic-focusing concept by using a double-pipe structure to produce titanium nanoparticles. Two immiscible fluids were led through the inner and outer tubes of various diameters. Depending on the flow velocity and properties of the fluids, an annular flow, slug flow or a flow spreading the inner tube fluid was created. The desired stable annular flow was achieved at low relative velocities between the two fluids. In this manner, the microspace between the two fluids used for nanoparticle synthesis was manipulated. SEM and TEM images revealed that uniform titanium particles were produced. Particle size increased with the inner tube diameter. The particles could easily be handled since no confined space was needed for particle synthesis and the outer fluid prevented any particle–wall contacts. The authors also claim that the device was advantageous due to easy maintenance and a low-priced setting.[42] Another example of a successful implementation of the hydrodynamic focusing concept was given by Génot *et al.*[44] They employed a 3D focusing device for the anti-solvent crystallization of rubrene.

Werner *et al.*[45] used two different mixer designs to investigate the potential suitability of precipitation reactions, both adopting the hydrodynamic-focusing principle. In an impinging jet mixer two fluid jets collide at a specific angle in the center of a mixing chamber. A gaseous or liquid stream surrounding the collision point hinders any particles formed from impinging on the wall. Stable jets required a certain minimum flow rate, a stable Y-jet being the preferred flow for precipitation reactions. Increasing the flow rate enhanced turbulent flow, and therefore the mixing quality, until a constant value was reached. The second mixer was a separation layer micromixer: inert solvent layers were introduced between the reacting fluids to shift the reaction and accompanying precipitation away from the multichannel feeds to larger mixing channels. This type of mixer required a laminar flow regime. Metallo-organic reactions and processes using auxiliary bases (*e.g.* amide formation) were considered. Three of the processes were used to evaluate both mixing concepts. The reactions could not be carried out in standard micromixers due to blocking within a few seconds. Although intense precipitation occurred

during the experiments, a continuous-flow process was established. The authors stated that the impinging jet mixer offers the most robust processing and best performance, whereas the separation layer mixer required more precise fluid control.[45]

The impinging jet mixer was also used by Grundemann *et al.*[46] for a continuous ink mixing process. Agglomerates may form if the induced mixing energy is too low. These agglomerates tended to deposit inside other mixing devices and in downstream equipment, eventually leading to plugging. However, the induced mixing energy was high enough to prevent the formation of agglomerates when an impinging jet mixer was used. A stable ink production process was therefore realized and in-spec ink was produced.[46]

A microreactor for fine particle production that is similar to the separation layer micromixer was developed by Nagasawa and Mae,[47] in the form of an annular multi-lamination microreactor. The reaction section was designed such that five annular layers of different fluids were formed, which were injected into the mixing and reaction zones as annular lamellar segments. Mixing was promoted by contracting channels that reduced the diffusion distance. The outermost and innermost lamellae serve as protection layers of the three streams in the middle and may also help to transport the fluids through the pipe in case of highly viscous reactants. If inert fluids are used, they will then prevent any wall contacts by the synthesized particles. A stable continuous crystallization of silver halide was demonstrated.[47]

Another way to avoid particle–wall contacts is to encapsulate precipitated particles by droplets, which are immiscible in the surrounding fluid. Shestopalov *et al.*[48] demonstrated this microfluidic method for the synthesis of colloidal cadmium selenide nanoparticles. Using microfluidic devices made of PDMS with channels of 50 μm height and 50 μm width, two aqueous reagents were separated by an inert fluid. The latter was used to prevent mixing between the two reagents until they had flown into a water-immiscible fluorinated oil phase to form droplets. The droplets were then transported by the oil phase through a number of winding channels allowing for mixing by chaotic advection and consequently for the reaction inside the droplets. A second reaction step was initiated by injecting a third reagent directly into the droplets. For mixing and reaction, another winding passage followed the merging junction. Only a negligible build-up of particles was found at the merging junction, and no particles adhered to the channel walls during 30 min.

Poe *et al.*[49] also investigated disperse-phase droplets as individual reactors and transport means to inhibit fouling during indigo synthesis. Their device was composed of syringe pumps, syringes, needles and laboratory tubing. A fluid inlet was created by inserting a needle with an inner diameter of 0.15 mm (outlet of the syringe) into the tubing. An inert carrier fluid was used as the continuous phase. Several reacting streams were inserted as droplets downstream. Mixing was either initiated by collision of two different reagent droplets or by diffusion from the carrier into the disperse phase. Mineral oil, hexane and toluene were used as inert and available carrier fluids. Using a mineral oil carrier phase, fouling inside the tubing was prevented.

Further work regarding droplet or segmented flow-based micro reactor designs that avoid particle–wall interactions to reduce fouling is reported widely.[50–54]

Electric field. Přibyl *et al.*[55] investigated clogging phenomena during precipitation experiments of calcium carbonate in microcapillaries. They controlled the precipitation process by imposing an electric field, avoiding unwanted clogging by the precipitate particles.

Choice of device materials. Schenk *et al.*[56] produced calcium carbonate by precipitation in different micromixers. Processing time was extended from 40 minutes with standard PTFE mixers to 5 hours when stainless steel micromixers were employed. The processing time was further doubled by applying indirect ultrasound during processing. They claim that controlled and precise dosing of reactants is vital to mitigate clogging of microstructured devices, too.[56]

Proper equipment design. During precipitation experiments, Kockmann *et al.*[2] detected fouling and blockages, especially downstream of the micromixer. They optimized the mixer design to minimize the surface area in contact with the particulate flow. In addition, the outlet channel, where fouling occurred mainly, was shortened. They concluded that well-designed micromixers can handle particulate flows, if the microstructured devices are tailored for the specific application.[3]

Wille *et al.*[5] also stated the importance of proper design for in- and outlet geometries to avoid the settling of particles. In their work azo-pigments were synthesized in a selection of different micromixers. Their mixing characteristics were first evaluated with the Villermaux–Dushman reaction. During synthesis with a caterpillar mixer the device was completely blocked, mainly due to the rectangular in- and outlet geometry of the device, as mentioned by the authors. As measures against blockage for processes involving particles or suspensions, they underline the importance of straight in- and outlet geometries so that particles cannot sediment.[5]

Researchers have also adapted process conditions to achieve low fouling tendencies: Hartman *et al.* performed a Pd-catalyzed C–N bond formation reaction in a microfluidic device with and without ultrasound. Without ultrasound, the formed particle sizes were on the same order as the channel dimensions (~400 μm), resulting in blocking. With ultrasound, the particle sizes decreased significantly, resulting in decreased fouling tendencies.[57,58] Similarly, Horie *et al.*[54] used ultrasound to inhibit the adhesion and sedimentation of precipitated particles in a micro reactor.

Sedelmeier *et al.*[59] stated that blocking issues could be solved for microstructured devices with a proper device design. They have validated that approach with several specifically designed reactors. However, they conclude that these solutions require specifically designed equipment and are of no use for standard commercial flow equipment. In their experiments, they used a T-mixer followed by a tube reactor with an inner diameter of 0.5 mm. However, stoichiometric quantities of manganese dioxide were formed during synthesis, which deposited in the reactor. This meant that the process had to

be regularly interrupted to enable cleaning of the T-piece connector. When the T-mixer along with a short length of the subsequent reactor tubing were placed inside an ultrasound bath, the aggregated manganese dioxide was effectively dispersed. As a result the mixture could be pumped as a suspension through the coil reactor with no adhesion or fouling, thus achieving a continuous flow process.[59]

Fouling mitigation during micro particle image velocimetry measurements. Micro particle image velocimetry (μ-PIV) is well-established for measurements of flow patterns in microstructured devices.[60,61] The fluorescent nanoparticles commonly used for the measurements tend to attach at microchannel walls, leading to erroneous information in the images and subsequent analysis.[62] Heinzel *et al.*[62] investigated fouling mitigation by agglomerate break-off upstream microstructured devices for μ-PIV applications. They identified that the absence of coalesced particles or agglomerates in the μ-PIV test device was significant for preventing fouling in microchannels. To disintegrate all agglomerates before entering the microstructured device, they added an ultrasound disintegrator, operated in the cavitation regime, with good performance.

Bridging. Hydrodynamic bridging, or blocking by arching,[63] occurs when particles flowing in a streamline make contact with each other,[4] see Fig. 4. This effect is quite similar to particle-based bridging in macroscopic silos (*e.g.* grain silos).

Bridging occurs when particles are growing in size or at constrictions, *i.e.*, at reduced flow path cross-sections. Wyss *et al.*[64] stated that clogging by bridging is based on the particle volume fraction. If the local particle concentration is large enough, bridging can occur. Also for systems with particle-to-particle or particle-to-wall repulsion, bridging can occur. In this case, a sufficiently high velocity is applied, which overcomes the interparticular repulsion forces, resulting in the formation of stable bridges.[4] The formation of bridges is expected for ratios of the flow characteristic path length to particle size of less than 3–4. Thus in practice, it is recommended that this ratio should be greater than 10.[4] Sharp and Adrian[63] investigated blocking of 75 μm to 400 μm glass capillaries by polystyrene latex particles, where the ratio was 3. They stated that blockage by bridging is a blocking mechanism (see Fig. 4) that has to be taken into consideration, especially for fouling in microchannels.[63]

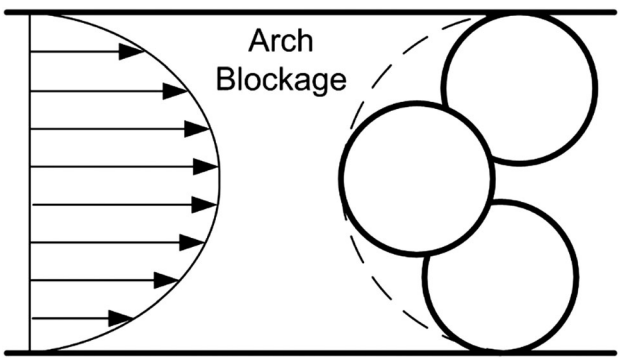

Fig. 4 Mechanism of bridging [modified[63]].

Another hint for bridging in micro dimensions was given by Georgieva *et al.*[65] They investigated the clogging of a ring-slit with highly concentrated latex dispersions (about 50 wt%). Against expectations, they showed that clogging of the ring-slit is independent of surface properties (hydrophilic *vs.* hydrophobic). This lead to the assumption that clogging of the ring-slit is not induced by particle deposition but by hetero-coagulation in the flow field at the slit entrance with impurities in the dispersions, supporting bridging due to higher particle/agglomerate diameters.[65] They showed that the blocking phenomenon depends on the flow rate. Small volumetric flow rates, resulting in small shear stresses, decreased the blocking tendency. This effect is also in accordance with observations by Hartman *et al.*[57] where decreased bridging tendency was attributed to lower shear stresses, as the particle–particle repulsive forces were dominant.

Random detachment. Hartman[4] also determined blocking *via* detached agglomerates from compounds formed at microreactor inlet header regions, which break off randomly due to shear stress. This results in microchannel blocking downstream in the microreactor itself, in transfer tubings or subsequent unit operations. Random detachment was also reported by Perry and Kandlikar.[33] They found relatively high standard deviations for pressure drop-based fouling investigations for silica dispersions. In three runs with identical conditions, the standard deviation was 60%. They showed interactions between fiber contaminations that were being caught at the entrance of microchannels, which acted like a filter for subsequently passing particles. Furthermore, they showed that lift forces in the microchannels, based on calculated shear stresses, are in the same order of magnitude as the gravitational forces. In contrast, the lift forces in the header regions of the micro device being used were smaller by two orders compared to the gravitational force, resulting in fouling and blocking mainly in the header regions. This led to a periodic break-off of particles/aggregates in the header regions upon entering the micro heat exchanger. Thus, high standard deviations of fouling experiments in microchannels can be explained by fouling in header regions and random break-off aggregates. Schenk *et al.*[56] investigated the precipitation of calcium carbonate in micromixers and expected a continuously increasing pressure drop. However, they found a constant pressure drop over long process times with sudden increases to a total blocking of the micromixers, which can be attributed to random detachment as well. Schoenitz *et al.*[66] also found random detachment as a predominant fouling mechanism during the continuous crystallization of lipid nanoparticles. The continuous crystallization was performed in a micro heat exchanger, with 32 parallel microchannels, each with a cross section area of 200 × 200 μm^2. Depending on formulation properties and especially the emulsifier concentration, the fouling behavior varies widely. With increasing emulsifier concentration the fouling tendency decreased, based on surface coverage of the solid lipid nanoparticles and thus increasing particle–particle repulsive forces. With decreasing emulsifier concentrations, increasing agglomerates attaching to the walls of the inlet header region were observed. The more agglomerates attached in the inlet header region, the more random detachment took place, leading to results with limited repeatability.

Biological growth fouling

Fouling layers composed of micro- or macro-organisms are classified as "biological growth fouling".[14] Aside from direct contamination from micro- or macro-organisms, their metabolic products and extra cellular polymeric substances, mainly proteins, can cause fouling issues in many applications. Applications affected include clinical monitoring, environmental monitoring and food quality control, either before or during processing.[67] These metabolic products are of great importance for lab-on-chip systems, *e.g.*, for blood analysis at point of care, and are essential for the buildup of biofilms. This chapter summarizes both topics: (i) biofouling based on the growth of micro-organisms, and (ii) fouling issues, which are directly related to microbial metabolic products that occur in microfluidic analysis systems. The specific process conditions and parameters, the fouling system, surface material, characteristic dimension and Reynolds number of published research concerning biological growth fouling are given in Table 4.

Ngene *et al.*[68] investigated the formation of biofilms upstream and downstream of membranes induced by freestanding structures, which act as spacers ($\sim$700 μm height) between different membranes and other surfaces. They investigated four different structure types experimentally and by CFD simulations. No relation between local wall shear stress and biofilm formation was found. They concluded that more comprehensive research is needed to correlate hydrodynamic conditions, micro-topology and biomass surface properties. To investigate the attachment and detachment of living cells in microfluidic-based lab-on-a-chip systems, Zhang *et al.*[69] introduced a new method. They investigated the influence of different surface modifications on the shear forces induced by increasing volumetric flow rates needed to detach living cells in microchannels. They also fitted the experimental data with a theoretical model, taking into account shear stress, surface adhesion bonds and hydrodynamic viscous stress. With this approach, different surfaces were investigated for their attachment/detachment behavior to a wide range of living cells in an easy and controlled fashion.

Schmolke *et al.*[70] investigated the detachment of living cells in microreactors. They used varying compositions of PDMS-based polyelectrolyte multilayers as surface coatings to create low-fouling surfaces in micro-bioreactors. They found that the adhesion strength of *S. cerevisiae* on different multilayer modifications was significantly reduced when compared to uncoated PDMS.

Bi *et al.*[71] described a modification of PMMA microchannels for bioanalysis. They stated that PMMA microchips are widely used to fabricate microfluidic devices because of their low cost, flexibility and ease of use in mass production, but have so far not been employed for biological applications due to hydrophobicity, poor biocompatibility and fouling (non-specific protein adsorption). They investigated a one-step procedure to create a hydrophilic surface on the hydrophobic PMMA substrate, resulting in low non-specific adsorption and thus low fouling.[71]

Lipscomb *et al.*[72] identified that the control of surface properties of glass-microchannels is a major parameter for preventing fouling of proteins on glass substrates. Patel *et al.* designed superhydrophilic surfaces for antifogging and anti-fouling investigations into microfluidic devices based on ITO-glass (indium tin oxide coated glass) and polyester.[73] The prepared surfaces showed a near-zero water contact angle (compared to 80° and 95° for the untreated surfaces). The adhesion of fluorescent proteins was investigated by fluorescence microscopy indicating a strong anti-fouling effect of the superhydrophilic surface for these proteins. Thus these surface modifications indicated potential for microfluidic devices. Helton *et al.* stressed the importance of pre-treating products processed in microchannels to prevent fouling issues.[74] They investigated chip-based micro total analysis systems (μTAS) for biomedical diagnostics of patient samples.[74] Biological contaminations due to mucins and proteins in the saliva led to fouling on the biosensor. Adequate pretreatment of saliva, filtering and H-filter extraction led to >90% less mucins and proteins and thus less fouling on the biosensor.[74] Um *et al.* described a method to avoid interactions between microchannel walls and biomaterials.[75] They encapsulated the living cells and proteins in hydrogel beads in a droplet-based micro reactor to minimize or avoid interactions between biomaterial and reactor walls.

Corrosion fouling

Corrosion in microstructured components is critical for the long-term stability of the devices themselves as well as the processes conducted therein due to three reasons. Firstly, the removal of small amounts of device material has a high impact on the internal geometries of microdevices with hydraulic diameters of often less than 1 mm. These dimensions are crucial for enabling improvements in heat and mass transfer compared to macrostructured devices. Adding extra material, *e.g.*, increasing the wall thickness, to limit the consequences of

Table 4 Experimental references for biological growth fouling in microstructured devices. Numbers in italics denote calculations performed by the authors, based on the information provided in the papers. d_h = characteristic dimension or channel dimensions, Re = Reynolds number

Ref.	Fouling system	Surface material	d_h [μm]	Re [—]
Lipscomb (2002)[72]	Proteins	Glass	*250*	*<10*
Bi (2006)[71]	Serum/plasma	PEG coated PMMA	50 × 120 × 3500	
Helton (2008)[74]	Human saliva	PMMA	62 × 3.6 × 60	0.4–4
Zhang (2008)[69]	Living cells	Coated glass substrates	60 × 320 × 2320	*<1*
Um (2008)[75]	Living cells, proteins	PDMS	90 × 50	*<1*
Ngene (2010)[68]	Biofilm solution	PMMA	Spacers: height of 700	83
Patel (2010)[73]	Proteins	Coated ITO glass		
Schmolke (2010)[70]	Yeast cells	Coated PDMS	120 × 4000 × 64 000	

corrosion is therefore counterproductive. Secondly, the dimensions of the internal structures are similar to the microstructures of the device material itself, rendering it susceptible to corrosion.[76] Thirdly, the material removed by erosion and/or corrosion products might become entrained with the fluid and deposit. This might result in fouling layers or complete blockages of the microstructures or the equipment downstream.

So far, no reports covering corrosion fouling in microstructured devices have been published, whereas papers covering the preliminary phenomena erosion[77–82] and/or corrosion[83–91] of microchannels exist. To give an overview of the investigations of these preliminary phenomena of corrosion fouling, Table 5 lists experimental reports of erosion and corrosion in microstructured devices stating the fluid or substance used, the surface material of the microchannel walls and the maximum duration of the experiments. All papers investigated erosion or corrosion phenomena based on devices that were taken out of service after several 1000 hours of operation. Thus, no time-dependent local erosion and corrosion investigations were possible and the published investigations are qualitative rather than quantitative.

As the prevention or mitigation of corrosion fouling and preliminary phenomena erosion and corrosion is a matter of the correct choice of material, several papers deal with selecting suitable materials for the process conditions.[76,87–89]

Clogging by gas bubbles

The unwanted accumulation of gas, especially air, in process equipment is a serious issue, regardless of the equipment's dimensions. It requires venting of these devices before processing. For microchannels, air bubble diameters are in the range of the characteristic dimension and are capable of blocking the whole cross section. This results in a complete blocking of the liquid flow in these microchannels, requiring high pressure gradients to move the bubbles.[92] This gives rise to an equivalent operational misbehavior of the affected devices as the above fouling categories. Thus "clogging by gas bubbles" was added to this review, since cross section area is decreased and the heat transfer is lowered for respective processes.

Clogging by gas bubbles particularly occurs while filling the microchannels at the start of an experiment.[3,93] Before starting an experiment, the microchannels usually contain air, which can lead to clogging of the micro device or single microchannels through air bubble entrapment. As the channels are filled with reactants during the process, this effect is commonly not induced in that case. During processing, another effect may however hinder the production: gas bubble clogging due to rapid coalescence and therefore growing gas bubbles. If the design of a device is based on internal numbering-up, *e.g.* multiple parallel microchannels within one micro device, blocking of single microchannels alters the internal geometry of the device. This may lead to flow maldistribution which may result in inhomogeneous product properties.[94] Furthermore, the flow resistance across the device/channel increases.[95] Also optical detection methods can be affected due to light reflections from entrapped air bubbles.[93] This chapter is divided into two parts: (1) gas bubble clogging during filling/priming of microchannels, and (2) gas bubble clogging due to rapidly growing gas bubbles during processing. Table 6 lists experimental reports of gas bubble clogging in microstructured devices stating the characteristic dimensions and Reynolds numbers of the experiments.

Gas bubble clogging during filling/priming of microchannels. In the initial state of experiments, the microchannels are filled with the process liquid without external forces. Therefore the surface tension of the liquid and the wetting characteristics of the microchannel wall material need to be adjusted such that microchannel filling, driven by capillary forces, takes place.

Table 5 Experimental references of erosion and corrosion in microstructured devices. Numbers in italics denote calculations performed by the authors based on the information provided in the papers. d_h = characteristic dimension or channel dimensions, t = maximum duration of experiment

Ref.	d_h [μm]	Fluid/medium	Surface material	t [h]
Bowers (1994)[78]	510	R-113	Metallic surfaces	
Ferstl (2004)[88]		Concentrated sulphuric acid, fuming nitric acid	Several metals, PTFE, PFA, silicon, Si_3N_4, SiO_2	
Treusch (2005)[80]	*300*	Filtered tap water	Copper	1000–10 000
Kockmann (2005)[3]		Water	Alumina foil	50
Wright (2006)[90]		Decomposition environment of sulfuric acid (>900 °C)	Different sintered materials	100, 200, 500, 1000
Daymo (2007)[82]		Combustion conditions	Alloy 617 (coated)	4000
Lee (2007)[77]	821 × 215 × 44 800	Nanofluid containing Al_2O_3	Copper for microgrooves, polycarbonate	30/94
Feeler (2008)[81]		Water	Copper, ceramic	550–2500
Karni (2008)[83]		Filtered tap water, deionized water	Copper	500–1000
Balsley (2009)[84]		Deionized water	Copper, surfaces were Au plated	1000–5000
Jackel (2011)[85]	*150–300*	Filtered, deionized, deoxygenated water; 10% acetic acid	Copper with Au coating	
Makarshin (2011)[91]	*50*	*Catalytic partial oxidation of methane*	FeCrAl	
Eichhorn and Gietzelt (2012)[76]		*Hot sulfuric acid (95–97% at 100 °C/50% at 125 °C)*	Nickel-based alloy and glassy carbon (Sigradur® G)	*336/1008*
Bonner (2012)[79]		Deionized water, salt water solution	Copper, gold-plated copper, aluminia/Au plated	
Gietzelt (2013)[89]	*300*	Hot sulfuric acid (95–97% at 100 °C)	Hastelloy	1000

Edges are preferentially wetted prior to plane microchannel walls, which results in a splitting of the fluid in micro cavities at cross-sectional extensions and gas inclusions as illustrated in Fig. 5.[3,93]

Goldschmidtböing *et al.*[93] identified this process of air entrapment by an unstable meniscus as the predominant mechanism for the formation of air bubbles in microstructured devices. Capillary and viscous forces dominate while filling the microchannels. Based on numerical simulations, they provide design rules which are independent from experimental fits and can hence be applied to identify "filling-friendly" microfluidic structures.[93]

Tseng *et al.*[96] investigated the surface tension-driven filling (*i.e.*, capillary filling) of microchannels with integrated reservoirs of specific shapes. The reservoirs had rectangular or 45° shapes. Both the microchannel as well as reservoir surfaces were modified. This led to different hydrophilic/hydrophobic properties and varying contact angles between the process fluid and the surface. Reynolds numbers were approximately 0.002. Complete filling of the reservoirs failed for all tested surface modifications, which accorded with the results of the numerical simulations. Integrated reservoirs or any kind of microchannel enlargement led to different pressure barriers for the fluid flow.

Man *et al.*[97] calculated these pressure barriers for differently shaped microchannel enlargements. If a fluid passes these enlargement regions, the capillary forces have to exceed the pressure barriers. External pressure can be used to overcome the pressure barrier, which can be provided by heating or electrolytic generation of O_2 bubbles in the liquid phase.[97]

Kim *et al.*[98] investigated the surface tension during filling under varying inlet pressure conditions with an array of 10 parallel microchannels of different widths ranging from 0.1 mm to 1 mm. In the narrowest microchannels, air blockages occurred, which they attributed to the negative effect of surface tension. At high inlet pressures, air got entrapped between the microchannel outlets due to dominating inertia forces. This effect was not detected at low inlet pressures because of the dominating viscous forces in this case.[99] The experimental results were verified by numerical simulations.

Jensen *et al.*[100] investigated clogging mechanisms by gas bubbles that depended on the pressure conditions within microchannels to derive design rules for their construction at low clogging pressures. The clogging pressure is defined as the pressure at which a clogging gas bubble is pushed out of the microchannel.[100] The smaller the clogging pressure, the easier it is to wash-off clogging gas bubbles. Their numerical simulations were based on geometry parameters like the angle of the constriction, the contact angle and the initial bubble length.[100] Kim and Whitesides[99] investigated the influence of varying surface properties on the macroscopic front of the filling liquid. They filled rectangular capillaries with liquid prepolymers, which were then solidified by photopolymerization within seconds. This method revealed how filling structures of the liquid by microscopic methods depend on the applied self-assembled monolayers, which caused varying surface properties. In order to predict the clogging behavior of capillaries, Sesterhenn *et al.*[101] studied complex capillary networks by simulating their (self-)priming and emptying depending on inertia, friction, gravitation and capillarity.

In most cases, the clogging gas bubbles consist of air whose solubility is low in many priming liquids, specifically in water. Taking this into account, Zengerle *et al.*[102] proposed a new method for gas bubble free-priming of microchannels: before priming microchannels, they replaced contained air (O_2–N_2 mixtures) with CO_2 whose solubility is 30-fold-higher in water compared to air. Hence, gas bubbles are not washed off due to high pressures, and instead they are dissolved in the priming liquid. This method is also useful for priming dead-end microchannels. However, carbon dioxide priming before experiments requires an extra purging step making experiments less user-friendly and more complex.[102] Steinert *et al.*[103] therefore presented special designs of dead-end microchannels which also allowed for bubble-free capillary filling.

Gas bubble clogging during processing. Once the process is operating, clogging by gas bubbles may be caused by rapidly growing gas bubbles, gas emissions of the fluid due to reactions, degassing downstream of pressure reductions or an unintentional wash-in of gas bubbles. In this case, the mobility

Table 6 Experimental references of gas bubble clogging in microstructured devices. Numbers in italics denote calculations performed by the authors based on the information provided in the papers. d_h = characteristic dimension, Re = Reynolds number

Ref.	d_h [μm]	Re [—]
Gravesen (1993)[105]		
Zengerle (1995)[102]		
Kim (1997)[99]	*0.7–1.4*	*Capillary filling*
Man (1998)[97]	*33*	
Sesterhenn (1999)[101]		*Capillary filling*
Tseng (2002)[96]	*Microchannels: 83 reservoirs: 200*	0.002 (*capillary filling*)
Kim (2002)[98]	*1000 to 100*	
Kohnle (2002)[92]	*583 + 150*	*8–420*
Goldschmidtböing (2003)[93]	*230*	
Jensen (2004)[100]	*Numerical simulation*	
Steinert (2004)[103]	*29 different geometries*	
Kockmann (2005)[3]		
Meng (2007)[95]		
Litterst (2008)[104]	*460*	
Maikowske (2010)[94]	*133*	

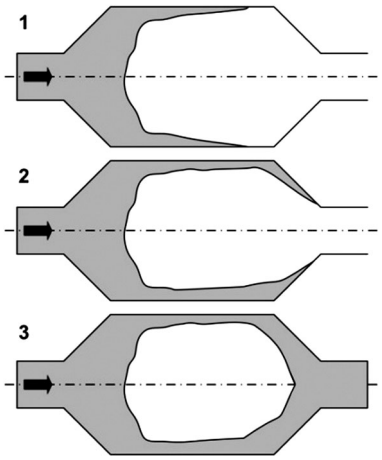

Fig. 5 Mechanism of gas inclusion *via* an unstable meniscus in micro cavities or cross-section extensions [adapted[3]].

of gas bubbles in the microchannel should be high in order to wash them off as fast as possible. Aiming at maximum bubble mobility, Litterst *et al.*[104] investigated an optimized design of T-shaped microchannels. They presented a method enabling the user to assess whether or not a T-shaped microchannel will be subject to gas bubble clogging or not. The dimensionless maximum velocity of gas bubbles in a given setup is introduced to describe the tendency for bubble movement, hence the tendency for clogging by gas bubbles. Their presented graphs can be used to design non-clogging T-shape microchannels with height to width ratios of 0.2–5.[104] Once gas bubbles have formed, the pressure drop across the microchannel acts as a driving force to wash them out. Gravesen *et al.*[105] listed equations to determine the pressure difference needed to transport gas bubbles in straight channels. For a water-filled capillary of 1 μm diameter, for example, 1.4 bar are needed. Kohnle *et al.*[92] also investigated a special channel geometry, the so-called ''channel at channel'', to prevent gas bubble clogging of microchannels. These rectangular microchannels consisted of one large microchannel with an extra small microchannel on the side leading to different capillary pressures. This arrangement forced the gas bubbles to move into one of the microchannels whereas the fluid bypasses this channel through the free microchannel, thus avoiding clogging of the whole cross section. Furthermore, the velocity in the free microchannel is increased causing a higher pressure drop on the gas bubble side and therefore an increased gas bubble mobility.[92]

Gas bubble clogging is of special interest at evaporation processes in microchannels, especially when the flow velocity is too low to wash off all generated gas bubbles. Maikowske *et al.*[94] investigated vapor clogging and slugging phenomena which occur during water evaporation in microchannel arrays. They observed two different types of vapor clogging: vapor plugging at channel inlets and inside the microchannels. Different vapor clogging phenomena led to flow maldistributions and hence to inhomogeneous vapor quality at the vapor outlet of microchannel arrays.[94]

Meng *et al.*[95] stated that methods like ''bypassing'', ''trapping'' and ''special shapes'' of microchannels can tolerate limited amounts of gas within the microchannels, but do not solve the bubble clogging problem itself. If gas is generated constantly during processing, efficient gas removal out of the microchannels is needed. Therefore, Meng *et al.*[95] employed microscopic hydrophobic capillaries encased by hydrophobic nanoporous membranes. Gas bubbles are removed through these hydrophobic capillaries while the liquid is retained by the hydrophobic membranes from flowing out.[95]

Taking air bubble clogging into account, a modification of the fouling definition especially for microchannels seems meaningful. Reformulating this definition in a broader sense to the ''unwanted accumulation of material affecting heat, mass and/or momentum transport'' instead of ''unwanted deposition on surfaces'' would also include air bubble clogging as a fouling phenomenon in microchannels.

Analogies and differences of fouling in micro- and macrostructured devices

Conducting chemical processes in microstructured rather than macrostructured devices results in altered geometrical and flow conditions, which also affect the fouling behavior of these devices. The differences are (i) the characteristic inner tube/channel diameter is smaller than 1 mm, whereas in macro equipment dimensions of more than 10 mm are typically applied, (ii) this results in a surface-to-volume ratio of up to 100 000 m^2 m^{-3}, more than 100 times higher than for macro structured devices, and (iii) the flow regime is usually laminar.

At these typical laminar flow regimes in micro devices paired with low wall shear stress affecting the fouling layers, fouling build-up increases whereas the detachment of matter decreases. Therefore, microchannels are very prone to fouling and complete blockages, resulting in maldistribution of the fluid flow in parallel channels. Blocked channels also cause altered cleaning mechanisms compared to non-blocked channels, as Schoenitz *et al.*[106] point out: in ''*non-blocked microchannels, cleaning is induced by wall shear stresses. In contrast, blocked microchannels lead to dead zones up-stream of the blocked areas, resulting in pressure forces instead of shear stresses. Thus especially for these blocked channels, chemical cleaning becomes more important*''.[106]

In operating microstructured devices a capturing effect has also been observed.[66,107] The effect is due to porous fouling layers with internal pores of various sizes acting as obstacles for particles or agglomerates, which have been detached upstream of the pore system. Blockages may then occur as a consequence of this capturing effect and may consequently be attributed as secondary fouling. Primary fouling, on the other hand, is based on particle–wall or particle–particle adhesive forces. In macrostructured equipment, secondary fouling is very rare since the characteristic dimensions are much larger. If such pronounced fouling layers were to occur in macrostructured equipment, heat transfer and pressure drop would suffer to such an extent that a cleaning cycle would be started before secondary fouling occurred.

Heat exchanger fouling. Heat transfer is a frequently used unit operation in process engineering, thus fouling investigations in heat exchangers are widespread, no matter the underlying dimension. In micro heat exchangers, the predominant

fouling types are crystallization and particle fouling. For these fouling types, Schoenitz *et al.*[107] and Mayer *et al.*[22] found qualitatively similar trends to what is known for macroscopic dimension for the thermal fouling resistance and the pressure drop during continuous processing in microstructured devices. During continuous processing of lipid nanoparticles in the micro heat exchanger, the thermal fouling resistance showed no initiation phase but went through a clearly developed induction phase with a subsequent layer growth phase.[107] The maximum value reached ($>10 \times 10^{-4}$ m^2 K W^{-1}) indicated severe fouling as defined for macro dimensions, see Table 2. In addition, the pressure drop across the micro heat exchanger developed similarly to that observed on macro dimensions.[107] In general, the development and the defined fouling phases known from macro dimensions also appear in micro dimensions, but the relevant time scales (minutes) are much shorter compared to macro dimensions (hours). These shorter characteristic time scales mainly arise due to significantly higher surface-to-volume ratios combined with characteristic dimensions in the micro scale, and thus small flow cross sections for microstructured devices compared with macro devices. This drastically increases possibilities for particle to wall attachment.

These short time scales for fouling events may also give rise to the observed absence of aging phenomena in microsystems. If encountered, fouling in microstructured devices requires immediate measures thus preventing any deposit from a long-term aging process.

Negative values for the thermal fouling resistance, *i.e.*, enhanced heat transfer, are reported at turbulent flow regimes in macro dimensions. This is attributed to roughness and constriction effects due to the fouling layers.[20] This effect was also observed by Schoenitz *et al.*[107] for micro devices, although at laminar flow regimes. In their investigations the maximum absolute values of thermal fouling resistance (thermal effect) and pressure drop (fluid dynamic effect of fouling) are much higher in micro dimensions, whereas the normalized increase of these fouling indicators is in the same order of magnitude compared to macro devices.[107] The "Degree of Fouling Increase" (DFI) may be employed for the comparison of fouling processes in micro and macro devices,[107] see eqn (5):

$$\mathrm{DFI} = \left| \frac{\frac{\Delta p_\mathrm{f} - \Delta p_0}{\Delta p_0}}{k_0 \cdot R_\mathrm{f}} \right| = \left| \frac{\Delta p^*}{\mathrm{Bi_f}} \right| \quad (5)$$

The equation relates the fluid dynamic effect of fouling (f = fouled; 0 = clean) to the thermal effect. The latter is expressed by the fouling Biot number, defined as the product of the overall heat transfer coefficient at the clean state k_0 with the thermal fouling resistance R_f. Micro systems with low fouling tendencies ($R_\mathrm{f} < 1 \times 10^{-4}$ m^2 K W^{-1}) are characterized by high DFI values since $\mathrm{Bi_f}$ values are low while Δp^* values are high due to fouling-based constriction effects. However, low fouling macro systems will show low DFI values. For systems with moderate or severe fouling tendencies, comparable DFI ranges can be found for micro and macro dimensions.[107] More experimental studies are necessary to investigate the DFI as a quantitative indicator to characterize differences in fouling between macro and micro dimensions.

Conclusions

This work provides a review on fouling research in microstructures. The majority of the reviewed papers may be grouped as follows: (i) intensified processes were described, resulting in higher yields or increased product properties compared to macro scale processing, (ii) fouling/blocking occurred during processing, and (iii) a solution to mitigate or prevent fouling altogether was developed for the specific process and microstructured device employed. Most of the presented papers offer very specific fouling investigations making it difficult to derive general rules and/or parameter dependencies, thus comparative or critical considerations of the reviewed papers are not possible. Thus, in the following a statistical approach was used to evaluate the research in the field of fouling in microchannels.

Traditionally, macro scale fouling phenomena can be classified based on Epstein's 5 × 5 matrix.[14] For fouling in micro dimensions, a sixth fouling category may be added to that matrix: clogging by gas bubbles. Although this type of clogging does not follow the macroscopic definition of fouling ("unwanted deposition on surfaces"), it results in comparable effects with respect to heat, mass and/or momentum transport to the affected devices. Thus, gas bubble clogging can be considered as a micro-specific fouling category, resulting in a 5 × 6 micro fouling matrix, see Fig. 6.

Following Wilson's approach to quantifying the research progress in macro scale fouling,[15] experimental-based papers (70 of all reviewed papers) dealing with fouling in microstructured devices were assigned to the respective fouling category as shown in Fig. 6.

In the first line, the number of papers assigned to the respective fouling category is indicated. In the lines below, the percentage of papers of a certain fouling category is stated

	1. Crystallization fouling	2. Particulate fouling	3. Chemical reaction fouling	4. Corrosion fouling	5. Biological fouling	6. Clogging by gas bubbles
Paper	**7**	**40**	**0**	**0**	**8**	**15**
Initiation [%]	43	35	0	0	75	60
Transport [%]	14	33	0	0	13	0
Attachment [%]	100	80	0	0	100	47
Removal [%]	29	43	0	0	13	80
Aging [%]	0	0	0	0	0	0

Fig. 6 Categories and sequential events of fouling in micro scale devices. In the first line, the number of papers assigned to the respective fouling category is indicated; in the other lines of a certain fouling category, the percentage of papers is stated in which this particular fouling event was addressed. Multiple occurrences were accounted for.

in which this particular fouling event was addressed. Multiple events were accounted for. It is obvious that the majority of papers within the 5 × 6 matrix were dealing with "particulate fouling". This is mainly due to the fact that microstructured devices offer great advantages specifically for reactions involving particle precipitation: based on intensified mixing on the micro-scale, the resulting particle size is decreased as well as the particle size distribution narrowed in many applications. Such reactions were among the very first examples studied in micro-structured devices and are still being investigated. As corrosion fouling is a matter of correct choice of material and oftentimes of long-term experiments, only papers dealing with the preliminary effects erosion and corrosion were found. Similar to this fouling category, the number of papers studying "clogging by gas bubbles" also was small. However, many papers dealt with the crystallization of solids, which were allocated to "particulate fouling". "Crystallization fouling" itself requires the formation of nuclei and their subsequent growth on the surface. Fouling due to biological systems in microstructured devices was studied only rarely, as biotechnological processes – aside from lab-on-a-chip or biomedical applications – just occasionally employ micro devices. The investigations mainly aimed at preventing fouling by observing and tackling the "initiation" and "attachment" phases are shown in Fig. 6. "Aging" of depositions in micro-structured devices was not addressed in any of the reviewed papers. This might be due to the fact that fouling in these dimensions is not tolerable for most applications, therefore processes are directly shut down when fouling occurs.

Revealing the fundamentals of fouling in microchannels, however, requires experimental studies of all sequential events and all influencing factors.

References

1 A. Stankiewicz, A. De Groot, H. Schoenmakers and H. Hanh, *Chem. Ing. Tech.*, 2007, **79**, 1362.
2 N. Kockmann, J. Kastner and P. Woias, *Chem. Eng. J.*, 2008, 110.
3 N. Kockmann, M. Engler and P. Woias, *Proc. of 6th HXFC*, 2005, p. 191.
4 R. L. Hartman, *Org. Process Res. Dev.*, 2012, **16**, 870.
5 C. Wille, H.-P. Gabski, T. Haller, H. Kim, L. Unverdorben and R. Winter, *Chem. Eng. J.*, 2004, **101**, 179.
6 E. F. C. Somerscale, *Heat Transfer Eng.*, 1990, **11**, 19.
7 R. Steinhagen, H. Müller-Steinhagen and K. Maani, *Heat Transfer Eng.*, 1993, **14**, 19.
8 M. Bohnet, *Chem. Eng. Technol.*, 1987, **10**, 113.
9 H. Müller-Steinhagen, *Adv. Heat Transfer*, 1999, **33**, 415.
10 H. Müller-Steinhagen, *Heat Exchanger Fouling*, PUBLICO Publications, Essen, 2000.
11 T. Geddert, W. Augustin and S. Scholl, *Chem. Eng. Technol.*, 2011, **34**, 1303.
12 A. P. Watkinson and D. I. Wilson, *Exp. Therm. Fluid Sci.*, 1997, **14**, 361.
13 W. Augustin, J. Zhang, I. Bialuch, T. Geddert and S. Scholl, *Chem. Ing. Tech.*, 2006, **78**, 607.
14 N. Epstein, *Heat Transfer Eng.*, 1983, **4**, 43.
15 D. I. Wilson, *Preface – Proc. of 8th HXFC*, 2009.
16 V. Hessel, S. Hardt and H. Löwe, *Chemical Micro Process Engineering – Fundamentals, Modelling and Reactions*, Wiley-VCH, Weinheim, 2004.
17 N. Kockmann, *Micro Process Engineering: Fundamentals, Devices, Fabrication and Applications*, Wiley-VCH, Weinheim, 2006.
18 C. Wiles and P. Watts, *Chem. Commun.*, 2011, **47**, 6512.
19 Y. H. Lin, S. H. Wang, C. C. Huang, H. C. Pai and K. L. Tung, *Proc. of IEEE International Ultrasonics Symposium*, 2010, p. 1043.
20 F. Albert, W. Augustin and S. Scholl, *Chem. Eng. Sci.*, 2011, **66**, 499.
21 J. J. Brandner, W. Benzinger and U. Schygulla, *Proc. of 7th HXFC*, 2007.
22 M. Mayer, J. Bucko, W. Benzinger, R. Dittmeyer, W. Augustin and S. Scholl, *Exp. Therm. Fluid Sci.*, 2012, **40**, 126.
23 J. Bucko, M. Mayer, W. Benzinger, W. Augustin, S. Scholl and R. Dittmeyer, *Chem. Ing. Tech.*, 2012, **84**, 491.
24 M. Mayer, J. Bucko, W. Benzinger, R. Dittmeyer, W. Augustin and S. Scholl, *Exp. Heat Transfer*, 2013, **26**, 487.
25 M. Mayer, J. Bucko, W. Benzinger, R. Dittmeyer, W. Augustin and S. Scholl, *Exp. Heat Transfer*, 2015, **28**, 222.
26 W. Benzinger, J. J. Brandner, U. Schygulla and K. Schubert, *Proc. of 7th HXFC*, 2007.
27 W. Benzinger, U. Schygulla, M. Jäger and K. Schubert, *Proc. of 6th HXFC*, 2005.
28 M. Heim, R. Wengeler, H. Nirschl and G. Kasper, *J. Micromech. Microeng.*, 2006, **16**, 70.
29 I. Bell and E. A. Groll, *Appl. Therm. Eng.*, 2011, **31**, 742.
30 D. Genovese and J. Sprakel, *Soft Matter*, 2011, **7**, 3889.
31 J. L. Perry and S. G. Kandlikar, *Proc. of 6th ICNMM*, 2008, p. 1741.
32 J. L. Perry and S. G. Kandlikar, *Proc. of 4th ICNMM*, 2006, p. 837.
33 J. L. Perry and S. G. Kandlikar, *Microfluid. Nanofluid.*, 2008, **5**, 357.
34 I. Chowdhury and S. L. Walker, *J. Colloid Interface Sci.*, 2012, **369**, 16.
35 T. Niida, Y. Kousaka and T. Furukawa, *Part. Part. Syst. Charact.*, 1989, **6**, 69.
36 S. G. Yiantsios and A. J. Karabelas, *J. Colloid Interface Sci.*, 1995, **176**, 74.
37 S. G. Yiantsios and A. J. Karabelas, *Chem. Eng. Sci.*, 2003, **58**, 3105.
38 S. G. Yiantsios and A. J. Karabelas, *Int. J. Multiphase Flow*, 1998, **24**, 283.
39 N. Shukla and K. H. Henthorn, *Microfluid. Nanofluid.*, 2009, **6**, 521.
40 J. Wagner and J. M. Köhler, *Nano Lett.*, 2005, **4**, 685.
41 W. Zhengying, C. Meng, L. Xia, T. Yiping and L. Bingheng, *Chin. J. Mech. Eng.*, 2012, **25**, 729.
42 M. Takagi, T. Maki, M. Miyahara and K. Mae, *Chem. Eng. J.*, 2004, **101**, 269.
43 B. Marmiroli, G. Grenci, F. Cacho-Nerin, B. Sartori, E. Ferrari, P. Laggner, L. Businaro and H. Amenitsch, *Lab Chip*, 2009, **9**, 2063.
44 V. Génot, S. Desportes, C. Croushore, J. P. Lefèvre, R. B. Pansu, J. A. Delaire and P. R. von Rohr, *Chem. Eng. J.*, 2010, **161**, 234.
45 B. Werner, M. Donnet, V. Hessel, C. Hofmann, N. Jongen, H. Löwe, R. Schenk and A. Ziogas, *Proc. of the 6th IMRET*, 2002, p. 168.
46 L. Grundemann, V. Gonschorowski, N. Fischer and S. Scholl, *J. Cleaner Prod.*, 2012, **24**, 92.
47 M. Nagasawa and K. Mae, *Ind. Eng. Chem. Res.*, 2006, **45**, 2179.
48 I. Shestopalov, J. D. Tice and R. F. Ismagilov, *Lab Chip*, 2004, **4**, 316.
49 S. L. Poe, M. A. Cummings, M. P. Haaf and D. T. McQuade, *Angew. Chem., Int. Ed.*, 2006, **10**, 1544.
50 R. Vacassy, J. Lemaitre and H. Hofmann, *AIChE J.*, 2000, **46**, 1241.
51 N. Jongen, M. Donnet, P. Bowen, J. Lemaitre, H. Hofmann, R. Schenk, C. Hofmann, M. Aoun-Habbache, S. Guillemet-Fritsch, J. Sarrias, A. Rousset, M. Viviani, M. T. Buscaglia, V. Buscaglia, P. Nanni, A. Testino and J. R. Herguijuela, *Chem. Eng. Technol.*, 2003, **26**, 303.
52 C. J. Gerdts, V. Tereshko, M. K. Yadav, I. Dementieva, F. Collart, A. Joachimiak, R. C. Stevens, P. Kuhn, A. Kossiakoff and R. F. Ismagilov, *Angew. Chem., Int. Ed.*, 2006, **45**, 8165.
53 K. I. Sotowa, K. Irie, T. Fukumori, K. Kusakabe and S. Sugiyama, *Chem. Eng. Technol.*, 2007, **30**, 383.
54 T. Horie, M. Sumino, T. Tanaka, Y. Matsushita, T. Ichimura and J. Yoshida, *Org. Process Res. Dev.*, 2010, **14**, 405.
55 M. Přibyl, D. Šnita and M. Marek, *Chem. Eng. J.*, 2005, **105**, 99.
56 M. Schenk, M. Donnet, V. Hessel, C. Hofmann, N. Jongen and H. Löwe, *Proc. of 5th IMRET*, 2001, p. 489.
57 R. L. Hartman, J. R. Naber, N. Zaborenko, S. L. Buchwald and K. F. Jensen, *Org. Process Res. Dev.*, 2010, **14**, 1347.
58 T. Noël, J. R. Naber, R. L. Hartman, J. P. McMullen, K. F. Jensen and S. L. Buchwald, *Chem. Sci.*, 2011, **2**, 287.
59 J. Sedelmeier, S. L. Ley, I. R. Baxendale and M. Baumann, *Org. Lett.*, 2010, **12**, 3618.
60 C. D. Meinhart, S. T. Wereley and J. G. Santiago, *Exp. Fluids*, 1999, **27**, 441.

61 C. Cierpka and C. J. Kähler, *J. Visualization*, 2011, **15**, 1.
62 V. Heinzel, A. Jianu and H. Sauter, *Heat Transfer Eng.*, 2007, **28**, 222.
63 K. V. Sharp and R. J. Adrian, *Microfluid. Nanofluid.*, 2005, **1**, 376.
64 H. M. Wyss, D. L. Blair, J. F. Morris, H. A. Stone and D. A. Weitz, *Phys. Rev. E: Stat. Phys., Plasmas, Fluids, Relat. Interdiscip. Top.*, 2006, **74**, 061402.
65 K. Georgieva, D. J. Dijkstra, H. Fricke and N. Willenbacher, *J. Colloid Interface Sci.*, 2010, **352**, 265.
66 M. Schoenitz, N. Warmeling, W. Augustin and S. Scholl, *Exp. Heat Transfer*, 2014, **27**, 376.
67 G. Kyriacou, P. Vadgama and W. Wang, *Med. Eng. Phys.*, 2006, **28**, 989.
68 I. S. Ngene, R. G. H. Lammertink, M. Wessling and W. G. J. Van der Meer, *J. Membr. Sci.*, 2010, **364**, 43.
69 X. Zhang, P. Jones and J. Haswell, *Chem. Eng. J.*, 2008, **135**, 82.
70 H. Schmolke, S. Demming, A. Edlich, V. Magdanz, S. Büttgenbach, E. Franco-Lara, R. Krull and C.-P. Klages, *Biomicrofluidics*, 2010, **4**, 044113.
71 H. Bi, S. Meng, K. Guo, Y. Chen, J. Kong, P. Yang, W. Zhong and B. Liu, *Lab Chip*, 2006, **6**, 769.
72 R. C. Lipscomb, J. Clemmens, Y. Hanein, M. R. Holl, V. Vogel, B. D. Ratner, D. D. Denton and K. F. Böhringer, *Proc. of 2nd IEEE-EMB*, 2002, p. 21.
73 P. Patel, C. K. Choi and D. D. Meng, *J. Lab. Autom.*, 2010, **15**, 114.
74 K. L. Helton, K. E. Nelson, E. Fu and P. Yager, *Lab Chip*, 2008, **8**, 1847.
75 E. Um, D. S. Lee, H. B. Pyo and J. K. Park, *Microfluid. Nanofluid.*, 2008, **5**, 541.
76 L. Eichhorn and T. Gietzelt, *Chem. Eng. Technol.*, 2012, **84**, 169.
77 J. Lee and I. Mudawar, *Int. J. Heat Mass Transfer*, 2007, **50**, 452.
78 M. B. Bowers and I. Mudawar, *J. Electron. Packag.*, 1994, **116**, 298.
79 R. W. Bonner, J. Weyant, E. Fleming and K. Lu, *Proc. of 28th Applied Power Electronics Conference and Exposition*, 2012, p. 498.
80 G. Treusch, R. Srinivasan, D. Brown, R. Miller and J. Harrison, *Proc. of SPIE*, 2005, vol. 5711.
81 R. Feeler, J. Junghans, G. Kemner and E. Stephens, *Proc. of SPIE*, 2008, vol. 6876.
82 E. A. Daymo, B. Yang, T. J. Mazanec, S. Perry, *ACS National Meeting Book of Abstracts, 234th ACS National Meeting*, 2007.
83 Y. Karni, G. Klumel, M. Levy, Y. Berk, Y. Openhaim, Y. Gridish, A. Elgali, M. Avisar, M. Blonder, H. Sagy and A. Gertsenshtein, *Proc. of SPIE*, 2008, vol. 6876.
84 D. R. Balsley, D. C. Dawson, R. Johnson and R. J. Martinsen, *Proc. of SPIE*, 2009, vol. 7198.
85 S. Jackel, A. Meir, Z. Horvitz, I. Moshe, Y. Shimoni, Y. Lumuer, R. Feldman, I. Hershko and Y. Pekin, *Opt. Laser Technol.*, 2011, **43**, 687.
86 R. R. Lima, L. F. Hernandez, A. T. Carvalho, R. A. M. Carvalho and M. L. P. da Silva, *Sens. Actuators, B*, 2009, **141**, 349.
87 D. L. Hennan, V. Srivastava, H. K. Taylor, M. R. Hale, D. E. Hardt and L. Anand, *J. Micromech. Microeng.*, 2009, **19**, 115030.
88 W. Ferstl, S. Loebbecke, J. Antes, H. Krause, M. Haeberl, D. Schmalz, H. Muntermann, M. Grund, A. Steckenborn, A. Lohf, J. Hassel, T. Bayer, M. Kinzl and I. Leipprand, *Chem. Eng. J.*, 2004, **101**, 431.
89 T. Gietzelt, L. Eichhorn and M. Zürker, *Galvanotechnik*, 2013, **1**, 220.
90 E. N. Wright, M. A. Wilson and C. A. Lewinsohn, *Proc. of AIChE annual meeting*, 2006.
91 L. L. Makarshin, D. V. Andreev, A. G. Gribovskyi and V. N. Parmon, *Chem. Eng. J.*, 2011, **178**, 276.
92 J. Kohnle, G. Waibel, R. Cernosa, M. Storz, H. Ernst, H. Sandmaier, T. Strobelt and R. Zengerle, *Proc. of 15th MEMS*, 2002, p. 77.
93 F. Goldschmidtböing, R. Schlosser, S. Schonhardt and P. Woias, *Proc. of 12th International Conference on Solid State Sensors, Actuators and Microsystems*, 2003, p. 1883.
94 S. Maikowske, J. J. Brandner and R. Lange, *Appl. Therm. Eng.*, 2010, **30**, 1872.
95 D. D. Meng, T. Cubaud, C.-M. Ho and C.-J. Kim, *J. Microelectromech. Syst.*, 2007, **16**, 1403.
96 F. G. Tseng, I. D. Yang, K. H. Lin, K. T. Ma, M. C. Lu, Y. T. Tseng and C. C. Chieng, *Sens. Actuators, A*, 2002, **97–98**, 131.
97 P. F. Man, C. H. Mastrangelo, M. A. Burns and D. T. Burke, *Proc. of MEMS*, 1998, p. 45.
98 D. S. Kim, K. C. Lee, T. H. Kwon and S. S. Lee, *J. Micromech. Microeng.*, 2002, **12**, 236.
99 E. Kim and G. M. Whitesides, *J. Phys. Chem. B*, 1997, **101**, 855.
100 M. J. Jensen, G. Goranović and H. Bruus, *J. Micromech. Microeng.*, 2004, **14**, 876.
101 M. Sesterhenn, J. Mellmann, M. Löhr, B. Stierle, T. Strobelt and H. Sandmaier, *Proc. of MSM*, 1999, p. 538.
102 R. Zengerle, M. Leitner, S. Kluge and A. Richter, *Proc. of MEMS*, 1995, p. 340.
103 C. P. Steinert, H. Sandmaier, M. Daub, B. de Heij and R. Zengerle, *Proc. of MEMS*, 2004, p. 224.
104 C. Litterst, T. Metz, R. Zengerle and P. Koltay, *Microfluid. Nanofluid.*, 2008, **5**, 775.
105 P. Gravesen, J. Branebjerg and O. S. Jensen, *J. Micromech. Microeng.*, 1993, **3**, 168.
106 M. Schoenitz, W. Augustin and S. Scholl, *Proc. of Fouling and Cleaning in Food Processing*, 2014.
107 M. Schoenitz, J. H. Finke, A. Hohlen, N. Warmeling, C. C. Müller-Goymann, W. Augustin and S. Scholl, *Proc. HXFC X*, 2013.

